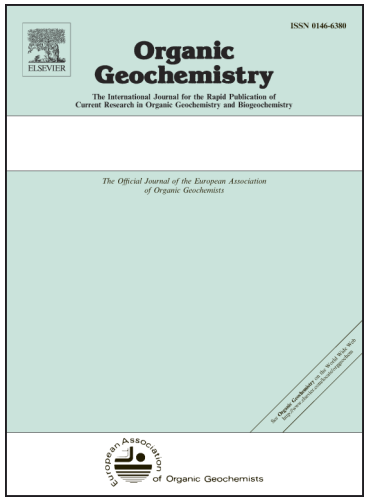

An improved method for the analysis of archaeal and bacterial ether core lipids

Kevin W. Becker, Julius S. Lipp, Chun Zhu, Xiao-Lei Liu, Kai-Uwe Hinrichs

PII: S0146-6380(13)00117-4
DOI: http://dx.doi.org/10.1016/j.orggeochem.2013.05.007
Reference: OG 2962

To appear in: *Organic Geochemistry*

Received Date: 29 January 2013
Revised Date: 24 May 2013
Accepted Date: 29 May 2013

Please cite this article as: Becker, K.W., Lipp, J.S., Zhu, C., Liu, X-L., Hinrichs, K-U., An improved method for the analysis of archaeal and bacterial ether core lipids, *Organic Geochemistry* (2013), doi: http://dx.doi.org/10.1016/j.orggeochem.2013.05.007

An improved method for the analysis of archaeal and bacterial ether core lipids

Kevin W. Becker*, Julius S. Lipp, Chun Zhu, Xiao-Lei Liu, Kai-Uwe Hinrichs

Organic Geochemistry Group, MARUM Center for Marine Environmental Sciences & Dept. of Geosciences, University of Bremen, 28359 Bremen, Germany

*Corresponding author. Tel.: +49 421 218 65703.

E-mail address: k.becker@uni-bremen.de (K.W. Becker).

ABSTRACT

In recent decades, microbial membrane lipids have become a focus of geoscientific research because of their proxy potential. The aim of this study was to develop new methods for ultra high performance liquid chromatography (UHPLC) separation of isomers of archaeal and bacterial membrane ether lipids, in particular glycerol dialkyl glycerol tetraethers (GDGTs), because of their tendency to co-elute with related but incompletely characterized derivatives. Our newly developed protocol, involving analysis using two Acquity BEH HILIC amide columns in tandem, enables chromatographic separation of several of these co-eluting compounds, such as the isoprenoid GDGT with four cyclopentyl moieties and other chromatographic shoulders often observed in GDGT analysis. Additionally, resolved peaks were observed for isoprenoid GDGTs, branched GDGTs and isoprenoid glycerol dialkanol diethers (GDDs); these have typically the same molecular mass as the corresponding major compound. Multiple stage mass spectrometry (MS^2) indicated that the shoulder peaks represent either regioisomers or other structural isomers with different ring or methyl positions. In some samples, these isomers can be even more abundant than their "regular" counterparts, suggesting that previously hidden clues regarding source organisms and/or community response to environmental forcing factors may be encoded in the distributions.

Keywords: HPLC-MS, qTOF, core lipids, GDGT, GDD, branched GDGT, isomerism, TEX_{86}, BIT-index

1. Introduction

Archaeal and bacterial glycerol ether lipids are widespread in marine and terrestrial environments (Schouten et al., 2000, 2002; Weijers et al., 2007; Lipp et al., 2008; Liu et al., 2012a). The prominent glycerol dialkyl glycerol tetraethers (GDGTs) and glycerol dialkyl diethers (e.g. archaeol) provide information on the biogeochemistry and microbial ecology of natural ecosystems in modern and in ancient environments (e.g. Hoefs et al., 1997; Hinrichs et al., 1999; Kuypers et al., 2001; Biddle et al., 2006; Lipp et al., 2008; Lipp and Hinrichs, 2009). The respective core glycerol ether lipids are preserved in sediments on geological timescales and enable study of past archaeal activity (e.g. Bolle et al., 2000; Kuypers et al., 2001). Core GDGTs are used for a variety of paleoceanographic proxies such as TEX_{86} for sea surface temperature reconstruction (Schouten et al., 2002). It utilizes isoprenoid GDGTs from planktonic archaea and is based on the observation that an increasing number of cycloalkyl moieties in the GDGT distribution corresponds to increasing mean annual sea surface temperature. Moreover, proxies for the reconstruction of soil input to the ocean (BIT index; Hopmans et al., 2004), mean annual air temperature (MAAT) and soil pH (Weijers et al., 2007) were developed on the basis of branched GDGTs (brGDGTs), which originate partly from anaerobic soil bacteria. These proxies, in particular for MAAT and soil pH reconstruction, measure the degree of methylation (MBT) and cyclization (CBT) of brGDGTs, respectively. Another ubiquitous series of ether lipids in marine sediments is glycerol dialkanol diethers (GDDs), which have recently been identified (Liu et al., 2012b). Due to their recent discovery, the exact source of these lipids and their biogeochemical significance, as well as their significance as biomarkers, requires further exploration.

Conventional analytical methods, in particular gas chromatography (GC), are unsuitable for direct analysis of GDGTs because they are non-volatile high molecular weight compounds. For a long time analysis had to target the GC-amenable products of the ether cleavage reaction (e.g. DeRosa et al., 1977; Michaelis and Albrecht, 1979). The introduction of protocols utilizing high performance liquid chromatography-atmospheric pressure chemical ionization-mass spectrometry (HPLC-APCI-MS) for direct analysis of GDGT core lipids (Hopmans et al., 2000) facilitated the identification and quantification of these compounds. More recently, modified protocols for this method have been published, which on the one hand improved analysis speed and reduced solvent amount (Escala et al, 2007; Schouten et al., 2007) and on the other hand improved the chromatographic separation of specific GDGT isomers (Zech et al., 2012; De Jonge et al., 2013). However, in many chromatograms, GDGT peaks still showed shoulders due to co-elution with largely uncharacterized compounds.

For example, lipids with the same molecular mass as the GDGTs used for TEX_{86}, but with slightly earlier elution times have been observed in different studies (Pitcher et al., 2009, 2011; Sinninghe Damsté et al., 2012). They tentatively represent GDGT isomers based on different combinations of biphytane chains in two basic steric arrangements (cf. Fig. 1 forstructures of isoprenoid GDGT and GDD isomers). With existing methods the similarity in the structures results in incomplete separation, so component quantification is problematic. In addition, detailed characterization of the compounds has not been performed. The lack of such knowledge is largely due to a lack of chromatographic resolution, which prevents the compounds being examined individually without co-elution using MS^2 experiments. Additionally, chromatographic shoulders can potentially affect quantification of proxies for both SSTs (TEX_{86}) and terrestrial input into the oceans (BIT index). In some soils and hot springs the shoulders on the isoprenoid GDGTs were even more abundant than the well-characterized GDGTs (Pitcher et al., 2009), indicating their proxy potential. In this study we present improved protocols for an increased separation of archaeal and bacterial membrane ether lipids and tentatively assign previously co-eluting compounds by way of APCI-MS^2 with ultra HPLC (UHPLC).

2. Material and methods

2.1. Sample collection, homogenization and extraction

Samples were collected during RV Meteor cruise M84/1 ("DARCSEAS 1") from different depositional environments (Table 1). Site GeoB15103 is in the eastern Mediterranean and the sample is from sapropel S1; site GeoB15104 is in the Sea of Marmara, representing a location with high terrestrial input and site GeoB15105 in the Black Sea represents a methane-rich site (Zabel et al., in 2013). After recovery, the samples were immediately frozen and stored at -80 °C until further treatment. In addition, biomass from the archaeal culture *Nitrosopumilus maritimus* was used. Growth conditions have been described by Könneke et al. (2005). Cells were harvested in the late exponential phase and stored at -20 °C.

All frozen sediment samples were homogenized at -198 °C using a Restek Cryomill, which was operated as follows: two cycles of pre-cooling for 2 min each, with a speed of the impactor of 5 impacts s^{-1} and homogenizing and fragmenting for 2 min with 25 impacts s^{-1}. Homogenized sediment samples and the archaeal biomass were spiked with an internal standard (C_{46} GDGT; Huguet et al., 2006) and extracted, using a modified Bligh and Dyer protocol as described by Sturt et al. (2004). The wet weight of each sediment sample was 25 ± 0.5 g. The sediments were ultrasonically extracted (4 x 10 min) with CH_2Cl_2/MeOH/buffer (1:2:0.8, v:v:v) using 4

ml solvent g^{-1} sediment per extraction step. A phosphate buffer (8.7 g l^{-1} KH_2PO_4, pH 7.4) was used for the first two steps, and a Cl_3CO_2H buffer (50 g l^{-1}, pH 2) for the final two steps. After each step, the sample was centrifuged at 800 g for 10 min and the supernatant collected in a separation funnel. The combined supernatants were washed 3 x with deionized MilliQ water, allowing separation into an organic phase and a water-soluble phase, the organic phase being collected as the total lipid extract (TLE). The solvent was gentlyremoved under a stream of N_2 and the TLE stored at -20 °C.

2.2. Semi-preparative LC

In order to obtain cleaner fractions before further analysis, the TLE was subjected to semi-preparative HPLC for separation into an apolar fraction (containing core lipids) and a polar fraction (containing the more polar IPLs). A semi-preparative LiChrosphere Diol-100 column (250 x 10 mm, 5 µm, Alltech, Germany) was connected to a ThermoFinnigan Surveyor HPLC instrument equipped with a Gilson FC204 fraction collector. The flow rate was 1.5 ml min^{-1} and the eluent gradient was: 100% A to 65% B in 90 min, held at 65% B for 30 min, then 30 min column re-equilibration with 100% A, where A was *n*-hexane/isopropanol (90:10, v:v) and B isopropanol/MilliQ water (90:10, v:v). The apolar fraction was collected from 0 to 30 min and the polar fraction from 30 to 90 min. Solvent was removed under a stream of N_2 and the fractions stored at -20 °C until further analysis.

2.3. Hydrogenation

To ca. 10 mg PtO_2 in a homemade glass ampoule were added 50 µl *n*-hexane. The mixture was saturated with H_2 and a sample aliquot was added. After flushing with H_2, the ampoule was sealed and heated to 60 °C for 1 h. Finally, the sample was transferred to a 2 ml vial, evaporated to dryness and prepared for UHPLC-APCI-MS.

2.4. Methodology for GDGT analysis

Separation was carried out with a Dionex Ultimate 3000 UHPLC instrument. It was connected to a Bruker maXis ultra-high resolution quadrupole time-of-flight mass spectrometry (qTOF-MS) instrument, equipped with an APCI II source.

In order to test and validate various protocols for GDGT analysis, 10 µl aliquots in *n*-hexane:isopropanol (99.5:0.5, v:v) were injected onto different HPLC columns. The columns were: (i) a Prevail Cyano column (2.1 x 150 mm, 3 µm; Grace, Germany) maintained at 30 °C, (ii) a single Acquity BEH HILIC amide column (2.1 x 150

mm, 1.7 µm, Waters, Eschborn, Germany; cf. Wörmer et al., 2013) and (iii) two coupled Acquity BEH HILIC amide columns maintained at 50 °C. The solvent system and the gradients were adjusted for the BEH HILIC amide columns. Each sample was injected at least in duplicate, all samples analyzed according to the newly proposed protocol involving two coupled columns in triplicate

With the Prevail Cyano column, GDGTs were eluted using the following gradient (Liu et al., 2012b; modified after Schouten et al., 2007) with eluent A [*n*-hexane:isopropanol (99:1, v:v)] and eluent B [*n*-hexane:isopropanol (90:10, v:v)] at 0.2 ml min^{-1}: 100% A, held isocratically for 5 min, linear gradient to 90% A and 10% B in 20 min, followed by a linear gradient to 100% B at 35 min and then held isocratically at 100% B for 10 min. Cleaning the column was achieved by back flushing with 100% B for 5 min at 0.6 ml min^{-1}. Finally, the column was equilibrated with 100% A for 10 min.

With the Acquity BEH HILIC amide column (single and tandem), GDGTs were eluted using the following gradient with eluent A (*n*-hexane) and eluent B [*n*-hexane:isopropanol (90:10, v:v)] and a constant 0.5 ml min^{-1}: linear gradient from 3% B to 5% B in 2 min, linear gradient to 10% B in 8 min, linear gradient to 20% B in 10 min, linear gradient to 50% B in 15 min and linear gradient to 100% B in 10 min. In order to clean the column(s), 100% B was held for 6 min. Finally, the column(s) was/were equilibrated with 3% B for 9 min before the next injection. For all methods described above an UHPLC instrument is not necessarily needed because the LC pump pressure was generally below the maximum pressure allowed for many commonly used HPLC pumps.

Detection of GDGTs was achieved using positive ion APCI, while scanning a *m/z* range from 150 to 2000; source parameters were optimized during infusion of a mixture of GDGTs and finally were as follows: corona current 3500 nA, nebulizer gas 5 bar, drying gas 8 l min^{-1}, drying gas 160 °C, vaporizer 400 °C. The same APCI settings were used for all columns tested. Only the scan rate needed to be adjusted because the peak width differed strongly between the different methods tested, while we opted to obtain 20 to 30 scans per peak. The scan rate for the analysis with the Prevail Cyano column was 1 Hz and for the Acquity BEH HILIC amide column(s) 2 Hz. MS^2 spectra of GDGT and GDD compounds were obtained in data dependent mode. For each MS full scan, up to three MS^2 experiments targeted the most abundant ions with N_2 as collision gas and a collision energy of 53 eV for isoprenoid GDGTs and GDDs and 45 eV for brGDGTs, respectively. The isolation width was 9 Da. Active exclusion limited how often a given ion was selected for fragmentation and thus allowed us to obtain MS^2 data for less abundant ions. The mass spectrometer was set to a resolution of 27000 (at *m/z* 1222) and exact mass calibration was performed by loop-injection of tune mixture at the end of each run. Additionally,

every spectrum was corrected using a lock mass (*m/z* 922.0098), resulting in a final mass accuracy of typically < 1 ppm.

The chromatographic separation of individual protocols was validated on the basis of chromatographic resolution (Rs), which was calculated with Eq. 1 from the retention time difference of two adjacent peaks (ΔtR) divided by sum of their mean peak width at half peak height (W_{avg}):

$$Rs = \frac{\Delta tR}{W_{avg}} \quad (1)$$

TEX^{H}_{86} values were calculated using the most recent definition and calibration for high temperature regions by Kim et al. (2010):

$$TEX^{H}_{86} = \log \frac{[GDGT-2]+[GDGT-3]+[Cren']}{[GDGT-1]+[GDGT-2]+[GDGT-3]+[Cren']} \quad (2)$$

TEX^{H}_{86} was suggested to be the most appropriate index for reconstructing SST for (sub)tropical oceans (Kim et al., 2010) and is therefore reported here in order to validate if the new methods give comparable results and to estimate the influence of the co-eluting shoulder peaks. In order to estimate the reproducibility of the analysis we regularly analyzed a pooled environmental sediment sample from the Peru Margin (ODP Leg 201, Site 1227A-2H2-65-75 cm, 8.05 mbsf, 2H5-83-93 cm, 12.43 mbsf, 3H2-55-65 cm, 17.15 mbsf, 11H2-118-128 cm, 92.72 mbsf, 13H3-0-15 cm, 113.60 mbsf; D'Hondt et al., 2003).

3. Results and discussion

A reconstructed base peak chromatogram and the associated reconstructed density map of the sample GeoB15103-2, 21-34 cmbsf from the eastern Mediterranean obtained from the analysis using two Acquity BEH HILIC amide columns in tandem are shown in Fig. 2. The detected compounds include the well-established isoprenoid GDGTs, brGDGTs, GMGTs (glycerol monoalkyl glycerol tetraethers) and several recently identified classes: isoprenoid GDDs, brGDDs, OH-GDDs, OH-GDGTs. To further differentiate multiple series of non-isoprenoid brGDGTs, we have adopted the nomenclature of Liu et al. (2012a) in order to distinguish the major brGDGTs with four to six methyls that are used in the BIT index (Hopmans et al., 2004) from less abundant,

chromatographically distinct compounds with higher or lower degrees of methylation, i.e. hybrid isoprenoid/branched (IB) GDGTs, overly branched (OB) GDGTs, andsparsely branched (SB) GDGTs.

3.1. Evaluation of different UHPLC-APCI-MS methods

The chromatographic resolution of critical GDGT and GDD pairs for the different methods is shown in Table 2. The use of a single Acquity BEH HILIC amide column showed considerable chromatographic improvement relative to the conventional protocol with the Prevail Cyano column, in particular for the GDDs. However, shoulder peaks were still not completely separated for the isoprenoid GDGTs. These promising results with this column, as well as its demonstrated utility for the analysis of intact polar lipids (Wörmer et al., 2013), led us to further invest time into optimizing its chromatographic separation. This resulted in a scheme with two Acquity BEH HILIC amide columns arranged in tandem, which vastly increased separation of the GDGT and GDD compounds (Fig. 3). One shoulder was baseline separated from GDGT-1, -2 and -3, respectively. These slightly earlier eluting compounds have the same molecular mass as each following GDGT and are therefore marked with an 'a'; for example GDGT-1a.

The tandem method also enabled separation of GDGT-4, which co-elutes with crenarchaeol (GDGT-5) with the conventional method. In the sediment samples the concentration of GDGT-4 was very low and it seemed to partly co-elute with crenarchaeol. However, the ion at *m/z* 1294 was slightly higher than the ion at *m/z* 1292 for the peak eluting just before crenarchaeol. Before this peak, an even smaller peak with a mass of 1294 Da eluted, which represents the chromatographic shoulder on GDGT-4. In order to further evaluate the separation of GDGT-4, the TLE of *N. maritimus* was analyzed. Here, the relative abundance of the compound eluting slightly before crenarchaeol was relatively high (Fig. 4a) and, based on the MS^2 spectra, was unambiguously assigned as GDGT-4 (Fig. 4b).

In addition to the increased separation, we compared injections of identical extract aliquots; the results showed strongly improved peak shapes for all modified protocols. For example, the mean peak width at half peak height of crenarchaeol was 0.251 min for the Prevail Cyano column and 0.091 min for the two Acquity BEH HILIC amide columns in tandem, resulting in higher sensitivity. Moreover, the 50 min analysis time for the new protocols was comparable with earlier methods using a single Prevail Cyano column (Hopmans et al., 2000; Schouten et al., 2007).

The two column protocol offers additional advantages for detection of brGDGTs and recently identified series of GDDs. Their chromatographic resolution was increased substantially (Table 2). For example, for each compound belonging to the group of GDDs, except for GDD-0, one shoulder was chromatographically separated. These peaks had the same molecular mass as the later eluting GDD (Fig. 3). The separated shoulders were designated with an 'a', for example GDD-1a. As for the group of isoprenoid GDGTs, the compound containing four cyclopentane moieties (GDD-4) was separated. Remarkably, the shoulder peaks of the GDDs were as abundant as their later-eluting counterparts. This is in contrast to the shoulder peaks of the isoprenoid GDGTs, which account for only ca. 10% compared with their counterpart. Among the brGDGTs, several previously co-eluting compounds with identical molecular mass were separated with the tandem method (Fig. 5). However, not all peaks could be baseline separated.

3.2. Assignment of unknown compounds

In order to study the fragmentation features of isoprenoid GDGTs, brGDGTs, as well as GDDs, in detail with exact mass and at high mass resolution, the samples were analyzed using UHPLC-qTOF-MS^2 to compare the MS^2 spectra of the GDGTs and their previously co-eluting shoulders.

3.2.1. MS analysis of isoprenoid GDGTs

MS analysis of GDGT-1 and the corresponding chromatographic shoulder (GDGT-1a) showed one main cluster of fragment ions in the MS^2 experiment (Fig. 6). Both precursor ions were $[M+H]^+$ at *m/z* 1300.3. The main MS^2 fragments in the cluster were *m/z* 741.7 and 557.6, resulting from the neutral loss of the acyclic biphytanyl moiety (Fig. 6). The enlarged spectra show that both fragmentation patterns were almost identical. Both spectra are characterized by multiple losses of water after loss of one biphytane moiety and glycerol-derived $C_3H_6O_2$ units. This fragmentation pattern is in agreement with the observation by Knappy et al. (2009, 2011) and Liu et al. (2012a), who discussed MS^2 spectra of tetraether core lipids in detail. The only slight difference between the spectra of GDGT-1a and GDGT-1 was the higher relative intensity of *m/z* 743.7 for the former, resulting from loss of a monocyclic biphytanyl moiety. Accordingly, GDGT-1 preferentially loses the acyclic biphytanyl moiety, while GDGT-1a does not show a preferential loss.

MS analysis of GDGT-2 and GDGT-2a ($[M+H]^+$ at *m/z* 1296.3) revealed similar patterns (Fig. 7). Here, the MS^2 fragments are formed from the loss of monocyclic alkyl chains (*m/z* 741.7; neutral loss 555.6 Da), indicative of

229 the presence of one cycloalkyl moiety in each biphytane chain. Interestingly, additional product ions resulting
230 from loss of alkyl chains containing zero (*m/z* 739.7; loss of 557.6 Da) and two (*m/z* 743.7; loss of 553.6 Da)
231 rings are also evident in the resulting MS^2 spectrum (Fig. 7).
232 The nearly identical mass spectra of the two GDGT pairs suggests that the core structures of GDGT-1 and
233 GDGT-1a, as well as GDGT-2 and GDGT-2a, are very similar. Possible structural differences are (i) double bonds
234 instead of cycloalkyl moieties, (ii) other structural isomers resulting from a combination of biphytanes with
235 different ring combinations, which can partially be resolved with MS data, e.g. zero ring/two ring or one
236 ring/one ring in case of GDGT-2 (Fig. 7), (iii) different ring positions within one biphytanyl moiety, or (iv)
237 regioisomers, i.e. isomers with parallel and anti-parallel arrangement of glycerol units, as for crenarchaeol and
238 its later eluting regioisomers (Sinninghe Damsté et al., 2002).
239 MS analysis cannot distinguish whether a double bond or a ring is present in the biphytane chain because it is
240 not fragmented at these positions. Furthermore, regioisomers and different positions of rings within one
241 biphytanyl moiety cannot be identified. However, such isomers could result in chromatographically separable
242 peaks.
243 In order to test for the presence of double bonds, an aliquot of the TLE was hydrogenated, but in no case did
244 the mass spectra or retention times of the components change. This suggested that the chromatographic
245 shoulders were not double-bond bearing compounds. Pancost et al. (2001), Schouten et al. (1998) and Knappy
246 et al. (2011) showed structural isomers for isoprenoid GDGTs, in which the position of rings differed, e.g. GDGT-
247 2 with an acyclic and a bicyclic biphytane moiety vs. GDGT-2 with two monocyclic biphytane moieties.
248 However, these isomers were not chromatographically resolved (Fig. 7) because both the major GDGT peaks
249 and the shoulder peaks showed mixed ring combinations in their MS^2 spectra, which excludes shoulder peaks
250 being such structural isomers. Therefore, these compounds represent either regioisomers or isomers with
251 different positions of rings within one biphytanyl moiety. Sinninghe Damsté et al. (2012) detected co-eluting
252 compounds in a thaumarchaeal soil isolate and suggested the compounds to be regioisomers. Theis
253 assumption was based on an earlier study by Sinninghe Damsté et al. (2002) who used NMR analysis to show
254 that compounds eluting later than the regular GDGTs 4 and 5 represent their regioisomers with a parallel
255 arrangement of glycerol units. GDGT-0, not associated with shoulders, appeared to be present as a single
256 structural isomer. Hence, for this compound the regioisomerism does not result in chromatographically
257 resolvable peaks using the commonly applied, as well as our newly implemented protocols. We cannot exclude

the separation efficiency of the tandem method still being insufficient for the separation of all isomers; alternatively not all possible combinations are necessarily present in nature. Further information on the nature of the less abundant shoulder peaks could be gained via chemical degradation, such as regiospecific ether cleavage. For example, Gräther and Arigoni (1995) showed that GDGT-0 from three archaeal species is in fact a 1:1 mixture of the regular, anti-parallel compound and its regioisomer with the parallel arrangement of glycerol units.

3.2.2. MS analysis of isoprenoid GDDs

MS analysis of GDDs and corresponding shoulder peaks revealed no discernible difference between the two groups, suggesting close structural similarity. All GDD MS^2 spectra were characterized by loss of one biphytanyl moiety, multiple losses of water and one glycerol-derived $C_3H_6O_2$ unit. For example, the main fragment ions for GDD-2, as well as for GDD-2a (each with the $[M+H]^+$ at *m/z* 1242.3), have *m/z* values of 667.6, 649.6, 631.6, 613.6, 593.6, 573.6 and 557.6/555.6 (Fig. 8); these ions are also observed during fragmentation of the isoprenoid GDGTs after they have lost one biphytanyl moiety and a $C_3H_6O_2$ unit. Regioisomerism can be excluded as a source of multiple peaks because GDDs contain only one glycerol. Therefore, the shoulder peaks must represent other structural isomers. Different biphytane moiety combinations can be excluded because they do not appear to be chromatographically resolved, e.g. fragments for both combinations, an acyclic and a bicyclic biphytane moiety vs. two monocyclic biphytane moieties, were observed in the spectra of GDD-2 and GDD-2a, indicating that the two peaks were mixtures of these two isomers. It remains to be resolved why only one shoulder peak was associated with each major GDD because, as for the isoprenoid GDGTs, for most GDDs several additional structural isomers are possible (see Fig. 1).

Interestingly, GDD shoulder peaks were relatively more abundant than the corresponding compound with the same molecular mass as the GDGT shoulder peaks in the three samples (Fig. 3, Table 4). The reason for this could be that, in the case of the GDGTs, the difference in polarity and/or steric configuration of some structural isomers with a different biphytane distribution is not large enough, leading to co-elution. For GDDs, however, where one glycerol unit is missing, a different biphytane distribution could result in larger differences that could be chromatographically well separated. This hypothesis could be tested in future studies employing NMR spectroscopy.

3.2.3. MS analysis of brGDGTs

A detailed analysis of mass spectra of brGDGTs was conducted on a purified brGDGT fraction of a sample from Aarhus Bay (56°07.06'N, 10°20.85'E, 15 m water depth, 6-7 m sediment depth). The fraction containing brGDGTs resulted as a byproduct from the OH-GDGT isolation (Liu et al., 2012b). We detected six distinct peaks (a-f) with similar fragmentation patterns in the EIC of m/z 1050.0, corresponding to brGDGT-III (Fig. 9). All MS^2 spectra showed a fragment ion resulting from the loss of a glycerol-derived $C_3H_6O_2$ unit (m/z 976.0; neutral loss of 74.0 Da), while the main cluster of fragments involved the loss of one alkyl moiety, multiple losses of water after losses of one alkyl moiety and glycerol-derived $C_3H_6O_2$ units. This fragmentation behavior is analogous to that of archaeal GDGTs (Knappy et al, 2009, 2011; Liu et al., 2012a) and has recently been described by De Jonge et al. (2013) for brGDGTs; these authors used a modified analytical set-up that resulted in improved chromatographic separation and the identification of four brGDGT-III isomers in a peat sample. Interestingly, all six peaks except peak f showed a mixed signal of at least two compounds, which differed in the total carbon number of the alkyl chains. Fragments reflect a brGDGT with a combination of two C_{31} alkyl chains and another one with a combination of one C_{30} and one C_{32} alkyl chain (Fig. 9, enlarged spectra), consistent with findings by De Jonge et al. (2013). The isomers we observed could either differ in the degree of methylation in the two C_{28} base alkyl moieties or the two linear base alkyl moieties were of different length, which would result in different degrees of methylation. Based on the MS^2 spectra we cannot distinguish such structural differences. The position of the methyls in the alkyl chains can also not be determined using MS^2 analysis but different methyl positions in the brGDGT molecule can result in chromatographically resolvable peaks (De Jonge et al., 2013). Nevertheless, our MS^2 experiments showed that the analyzed sample contains at least eleven brGDGT-III isomers, which cannot be chromatographically separated completely.

3.3. Validation of new protocols for determination of tetraether lipid proxies

The Peru Margin mix sample was analyzed during a three-month interval to estimate the reproducibility of the analysis. Results with the two-column protocol showed a standard deviation for the TEX^H_{86} of 0.0025 (relative standard deviation 0.72%). TEX^H_{86} values were calculated with and without chromatographic shoulders to evaluate the influence of incomplete separation, leading to possible overestimation of the peak area of individual GDGTs and therefore shifts in TEX^H_{86}. The calculated TEX^H_{86} values showed only minor differences between the different chromatographic methods, with a maximum difference of 0.03. This suggests that the

new methods are suitable for SST determination, but a larger set of samples needs to be analyzed to fully validate their applicability.

The impact of inclusion of shoulder peaks appears to be generally low but naturally increases with their relative abundance (Table 3). For the sample from site GeoB15103, with the highest relative abundance of shoulder peaks (Table 4), the maximum TEX^{H}_{86} discrepancy between inclusion vs. exclusion of shoulders was 0.07. For the other two samples, with relatively small shoulder peaks, the difference in the TEX^{H}_{86} value was 0.01. The small influence of co-eluting isomers on TEX^{H}_{86} values is consistent with earlier observations from an interlaboratory study by Schouten et al. (2009). However, the chromatographic shoulders can have an influence on the proxy when they are not separated and therefore included in the TEX_{86} calculation. In most commonly represented sediments, the abundance of the isomers is assumed to be low, but no study has focused on the quantification of these compounds in environmental samples.

The greater diversity of brGDGT isomers uncovered with the new protocol calls for further inspection and potential improvement in BIT index and CBT/MBT calculations since the specificity of selected isomers for the reconstruction process may be higher than that of the previously inseparable mixture.

4. Conclusions

The newly developed protocols, in particular the protocol using two columns in tandem, provides superior separation of archaeal and bacterial GDGT core lipids and opens a window to a more nuanced exploration of their distribution in the environment. The protocols feature reduced peak width at half peak height, higher peak height and thus increased sensitivity. Previously, partially co-eluting isoprenoid GDGTs can now completely separated and can be confidently quantified. Chromatographic shoulders were also separated within the group of the recently identified GDDs and, moreover, in the group of brGDGTs many additional peaks were revealed.

The exact structures of the compounds eluting as chromatographic shoulders of isoprenoid GDGTs and GDDs were not fully resolved. MS analysis showed the same fragmentation pattern for pairs comprising shoulder and major peak, suggesting a high degree of structural similarity. The substitution of cycloalkane moieties by double bonds in shoulder peaks was rejected on the basis of a hydrogenation experiment. Thus, the isomers of the GDGTs likely represent either regioisomers or structural isomers with different biphytane moieties; verification is needed, however, to support this hypothesis. Since regioisomers do not exist for GDDs, their

shoulder peaks must represent structural isomers, for example, isomers with exchanged biphytane chains or different ring positions within one biphytane chain.

Examination of MS^2 data for brGDGT-III isomers revealed similar fragmentation patterns for the six separated peaks and showed that most peaks were a mixture of isomers containing identical and different total carbon numbers in the two alkyl moieties. Therefore, the brGDGT isomers likely represent structural isomers with varying methyl positions and/or isomers with different base *n*-alkyl chain length. Identification of the exact structure of these isomers will be essential in future studies as the compounds may differ in their proxy potential, which could be further explored with the new protocol.

On a small set of samples we could show that the tandem method provides comparable TEX^{H}_{86} values as long as the chromatographic shoulder peaks were not included in the TEX_{86} in previous protocols.

Acknowledgements

We are grateful to the participating scientists and ship crews of the RV Meteor cruise M84/1 (DARCSEAS). We thank L. Wörmer for support with UHPLC. One sample for this study was retrieved during the Ocean Drilling Program (ODP) Leg 201. We also thank F. Elling and M. Könneke for providing biomass of *N. maritimus* and B. Orcutt for providing marine sediment from Aarhus Bay. The study was funded by the European Research Council under the European Union's Seventh Framework Programme - "Ideas" Specific Programme, ERC grant agreement # 247153 (Advanced Grant DARCLIFE; PI K.-U.H.) and by the Deutsche Forschungsgemeinschaft (DFG, Germany) through grants Inst 144/300-1 (LC-QTOF system), HI616/10-1 (K.-U.H.), LI1901/1-1 (J.S.L) and the postdoctoral fellowship granted through the Cluster of Excellence/Research Center MARUM to C.Z. Further support was given by the Bremen International Graduate School for Marine Sciences (GLOMAR) funded by the DFG. We thank two anonymous reviewers for helpful comments and suggestions.

Associate Editor - **S. Schouten**

References

Biddle, J.F., Lipp, J.S., Lever, M.A., Lloyd, K.G., Sorensen, K.B., Anderson, R., Fredricks, H.F., Elvert, M., Kelly, T.J., Schrag, D.P., Sogin, M.L., Brenchley, J.E., Teske, A., House, C.H., Hinrichs, K.-U., 2006. Heterotrophic archaea dominate sedimentary subsurface ecosystems off Peru. Proceedings of the National Academy of Sciences of the USA 103, 3846-3851.

372 Bolle, M.-P., Pardo, A., Hinrichs, K.-U., Adatte, T., von Salis, K., Burns, S., Keller, G., Muzylev, N., 2000. The
373 Paleocene-Eocene transition in the marginal northeastern Tethys (Kazakhstan and Uzbekistan). International
374 Journal of Earth Sciences 89, 390-414.

375 De Jonge, C., Hopmans, E.C., Stadnitskaia, A., Irene C. Rijpstra, W., Hofland, R., Tegelaar, E., Sinninghe Damsté,
376 J.S., 2013. Identification of novel penta-and hexamethylated branched glycerol dialkyl glycerol tetraethers in
377 peat using HPLC-MS^2, GC-MS and GC-SMB-MS. Organic Geochemistry 54, 78-82.

378 D'Hondt, S.L., Jørgensen, B.B., Miller, D.J. and Shipboard Scientific Party, 2003. Proc. ODP Init. Repts., vol. 201.
379 Ocean Drilling Program, Texas A & M University, College Station, TX.

380 DeRosa, M., DeRosa, S., Gambacorta, A., Minale, L., Bu'Lock, J.D., 1977. Chemical structure of the ether lipids of
381 thermophilic acidophilic bacteria of the Caldariella group. Phytochemistry 16, 1961-1965.

382 Gräther, O., Arigoni, D., 1995. Detection of regioisomeric macrocyclic tetraethers in the lipids of
383 Methanobacterium thermoautotrophicum and other archaeal organisms. Journal of the Chemical Society,
384 Chemical Communications, 405-406.

385 Hinrichs, K.-U., Hayes, J.M., Sylva, S.P., Brewer, P.G., De Long, E.F., 1999. Methane-consuming archaebacteria in
386 marine sediments. Nature 398, 802-805.

387 Hopmans, E.C., Schouten, S., Pancost, R.D., van der Meer, M.T.J., Sinninghe Damsté, J.S., 2000. Analysis of
388 intact tetraether lipids in archaeal cell material and sediments by high performance liquid
389 chromatography/atmospheric pressure chemical ionisation mass spectrometry. Rapid Communications in Mass
390 Spectrometry 14, 585-589.

391 Hopmans, E.C., Weijers, J.W.H., Schefuss, E., Herfort, L., Sinninghe Damsté, J.S., Schouten, S., 2004. A novel
392 proxy for terrestrial organic matter in sediments based on branched and isoprenoid tetraether lipids. Earth and
393 Planetary Science Letters 224, 107-116.

394 Huguet, C., Hopmans, E. C., Febo-Ayala, W., Thompson, D. H., Sinninghe Damsté, J. S., Schouten, S., 2006. An
395 improved method to determine the absolute abundance of glycerol dibiphytanyl glycerol tetraether lipids.
396 Organic Geochemistry 37, 1036-1041.

397 Kim, J.-H., van der Meer, J., Schouten, S., Helmke, P., Willmott, V., Sangiorgi, V., Koç, N., Hopmans, E.C.,
398 Sinninghe Damsté, J.S., 2010. New indices and calibrations derived from the distribution of crenarchaeal
399 isoprenoid tetraether lipids: implications for past sea surface temperature reconstructions. Geochimica et
400 Cosmochimica Acta 74, 4639-4654.

401 Knappy, C.S., Chong, J.P.J., Keely, B.J., 2009. Rapid discrimination of archaeal tetraether lipid cores by liquid
402 chromatography–tandem mass spectrometry. Journal of the American Society for Mass Spectrometry 20, 51-
403 59.

404 Knappy, C.S., Nunn, C.E.M., Morgan, H.W., Brendan, J.K., 2011. The major lipid cores of the archaeon
405 Ignisphaera aggregans: implications for the phylogeny and biosynthesis of glycerol monoalkyl glycerol
406 tetraether isoprenoid lipids. Extremophiles 15, 517-528.

407 Könneke, M., Bernhard, A.E., de la Torre, J.R., Walker, C.B., Waterbury, J.B., Stahl, D.A., 2005. Isolation of an
408 autotrophic ammonia-oxidizing marine archaeon. Nature 437, 543-546.

409 Kuypers, M.M.M., Blokker, P., Erbacher, J., Kinkel, H., Pancost, R.D., Schouten, S., Sinninghe Damsté, J.S., 2001.
410 Massive expansion of marine archaea during a mid-Cretaceous oceanic anoxic event. Science 293, 92-95.

411 Lipp, J.S., Morono, Y., Inagaki, F., Hinrichs, K.-U., 2008. Significant contribution of Archaea to extant biomass in
412 marine subsurface sediments. Nature 454, 991-994.

413 Lipp, J.S., Hinrichs, K.-U., 2009. Structural diversity and fate of intact polar lipids in marine sediments.
414 Geochimica et Cosmochimica Acta 73, 6816-6833.

415 Liu, X.-L., Summons, R.E., Hinrichs, K.-U., 2012a. Extending the known range of glycerol ether lipids in the
416 environment: structural assignments based on MS/MS fragmentation patterns. Rapid Communications in Mass
417 Spectrometry 26, 2295-2302.

418

419 Liu, X.-L., Lipp, J.S., Simpson, J.H., Lin, Y.-S. Summons, R.E., Hinrichs, K.-U., 2012b. Mono- and dihydroxyl
420 Glycerol Dibiphytanyl Glycerol Tetraethers in marine sediments: Identification of both core and intact polar
421 lipid forms. Geochimica et Cosmochimica Acta 89, 102-115.

422 Liu, X.-L., Lipp, J.S., Schröder, J.M., Summons, R.E., Hinrichs, K.-U., 2012c. Isoprenoid glycerol dialkanol diethers:
423 A series of novel archaeal lipids in marine sediments. Organic Geochemistry 43, 50-55.

424 Michaelis, W., Albrecht, P., 1979. Molecular fossils of archaebacteria in kerogen. Narutwissenschaften 66, 420-
425 421.

426 Pancost, R.D., Hopmans, E.C., Sinninghe Damsté, J.S., 2001. Archaeal lipids in Mediterranean cold seeps:
427 Molecular proxies for anaerobic methane oxidation. Geochimica et Cosmochimica Acta 65, 1611-1627.

428 Pitcher, A., Schouten, S., Sinninghe Damsté. J.S., 2009. In situ production of crenarchaeol in two California hot
429 springs. Applied and Environmental Microbiology 75, 4443-4451.

430 Pitcher, A., Hopmans, E.C., Mosier, A.C., Park, S.-J., Rhee, S.-K., Francis, C.A., Schouten, S., Sinninghe Damsté.
431 J.S., 2011. Core and intact polar glycerol dibiphytanyl glycerol tetraether lipids of ammonia-oxidizing archaea
432 enriched from marine and estuarine sediments. Applied and Environmental Microbiology 77, 3468-3477.

433 Schouten, S., Hoefs, M.J.L., Koopmans, M.P., Bosch, H.-J., Sinninghe Damsté, J.S., 1998. Structural
434 characterization, occurrence and fate of archaeal ether-bound acyclic and cyclic biphytanes and corresponding
435 diols in sediments. Organic Geochemistry 29, 1305-1319.

436 Schouten, S., Hopmans, E.C., Pancost, R.D., Sinninghe Damsté, J.S., 2000. Widespread occurrence of structurally
437 diverse tetraether membrane lipids: Evidence for the ubiquitous presence of low-temperature relatives of
438 hyperthermophiles. Proceedings of the National Academy of Sciences USA 97, 14421-14426.

439 Schouten, S., Hopmans, E.C., Schefuss, E., Sinninghe Damsté, J.S., 2002. Distributional variations in marine
440 crenarchaeotal membrane lipids: a new tool for reconstructing ancient sea water temperatures? Earth and
441 Planetary Science Letters 204, 265-274.

442 Schouten, S., Huguet, C., Hopmans, E.C., Kienhuis, M.V.M., Sinninghe Damsté, J.S., 2007. Analytical
443 methodology for TEX_{86} paleothermometry by high-performance liquid chromatography/atmospheric pressure
444 chemical ionization-mass spectrometry. Analytical Chemistry 79, 2940-2944.

445 Schouten, S., et al., 2009. An interlaboratory study of TEX_{86} and BIT analysis using high-performance liquid
446 chromatography-mass spectrometry. Geochemistry Geophysics Geosystems 10, Q03012.

447 Sinninghe Damsté, J.S., Hopmans, E.C., Pancost, R.D., Schouten, S., Geenevasen, J.A.J., 2000. Newly discovered
448 non-isoprenoid glycerol dialkyl glycerol tetraether lipids in sediments. Chemical Communications, 1683-1684.

449 Sinninghe Damsté, J.S., Schouten, S., Hopmans, E.C., van Duin, A.C.T., Geenevasen, J.A.J., 2002. Crenarchaeol:
450 the characteristic core glycerol dibiphytanyl glycerol tetraether membrane lipid of cosmopolitan pelagic
451 crenarchaeota. Journal of Lipid Research 43, 1641-1651.

452 Sinninghe Damsté, J.S., Rijpstra, W.I., Hopmans, E.C., Jung, M.Y., Kim, J.G., Rhee, S.K., Stieglmeier, M., Schleper,
453 C., 2012. Intact polar and core glycerol dibiphytanyl glycerol tetraether lipids of group I.1a and I.1b
454 thaumarchaeota in soil. Applied and Environmental Microbiology 78, 6866-6874.

455 Sturt, H.F., Summons, R.E., Smith, K., Elvert, M., Hinrichs, K.-U., 2004. Intact polar membrane lipids in
456 prokaryotes and sediment deciphered by high-performance liquid chromatography/electrospray ionization
457 multistage mass spectrometry-new biomarkers for biogeochemistry and microbial ecology. Rapid
458 Communications in Mass Spectrometry 18, 617-628.

459 Weijers, J.W.H., Schouten, S., van den Donker, J.C., Hopmans, E.C., Sinninghe Damsté, J.S., 2007. Environmental
460 controls on bacterial tetraether membrane lipid distribution in soils. Geochimica et Cosmochimica Acta 71,
461 703-713.

462 Wörmer, L., Lipp, J.S., Schröder, J.M., Hinrichs, K.-U., 2013. Application of two new LC-ESI-MS methods for
463 improved detection of intact polar lipids (IPLs) in environmental samples. Organic Geochemistry, 59, 10-21.

464 Zabel, M. (Eds.) (2013). Biogeochemistry and methane hydrates of the Black Sea; Oceanography of the
465 Mediterranean; Shelf sedimentation and cold water carbonates, Cruise No. 84/1, Febr. 9 - 22, 2011; La Valetta-
466 Istanbul. METEOR-BERICHTE.

467 Zech, R., Gao, L., Tarozo, R., Huang, Y., 2012. Branched glycerol dialkyl glycerol tetraethers in pleistocene loess-
468 paleosol sequences: Three case studies. Organic Geochemistry 53, 38-44.

469

470 **Figure captions**

Fig. 1. Structures of biphytanyl di- and tetraether membrane lipids. The basic structure of a GDGT is composed of two biphytanyl units X and Y, which may be interchanged with respect to their positions at sn-2 and sn-3 of glycerol. For the basic structure of a GDGT both the anti-parallel (A) and parallel configurations (B) are drawn. In addition, the basic structure of a GDD is shown, which is ether bound to isoprenoid chains containing 0 to 3 rings. The tables provide structural combinations for the different GDGT and GDD isomers arising from different biphytanyl moieties and, for GDGTs, from the parallel and anti-parallel configuration. Primed biphytanyl moieties (e.g., b') refer to the vertical mirror images of the non-primed versions shown. Only published and commonly detected biphytanes were taken into account for constructing possible isomer structures (Schouten et al. 1998,, 2000). More structural combinations are possible.

Fig. 2. (a) Reconstructed UHPLC-APCI-qTOF-MS base peak chromatogram showing isoprenoid GDGTs, brGDGTs, isoprenoid GDDs and OH-GDGTs in the core lipid fraction of M84/1 GeoB15103-2, 21-34 cmbsf. The sample was analyzed using two Acquity BEH HILIC amide columns in tandem; (b) associated, reconstructed density map plot showing the major diagnostic ions of all archaeal and bacterial ether lipids in the core lipid fraction. Also shown are representative structures of the different compound groups. Abbreviations (according to Liu et al., 2012a): GDGT, glycerol dialkyl glycerol tetraether; GDD, glycerol dialkanol diether; GMGT, glycerol monoalkyl glycerol tetraether; OH, monohydroxy; 2OH, dihydroxy; br, branched; IB, hybrid isoprenoid/branched; OB, overly branched; SB, sparsely branched; Unk, unknown.

Fig. 3. UHPLC-APCI-MS chromatograms, shown as extracted ion chromatograms (EICs), illustrating isoprenoid GDGTs and GDDs in the apolar fraction of sample M84/1 GeoB15103-2, 21-34 cmbsf. Compounds labeled with an 'a' have the same molecular mass as the corresponding, later eluting compound. Numbers represent numbers of unsaturation (rings and/or double bonds). Chromatographic separation was greatly increased for the GDGTs and GDDs when two Acquity BEH HILIC amide columns in tandem were used. For further explanation, see text.

Fig. 4. (a) UHPLC-APCI-MS chromatogram, shown as extracted ion chromatogram (EIC), illustrating the isoprenoid GDGTs in the TLE of the archaeal culture *N. maritimus*; (b) product ion (MS^2) spectra of GDGT-4 ($[M+H]^+$ ion of *m/z* 1294.3, in the range *m/z* 540-1320), show the diagnostic product ions used to assign the structure. The major fragments at *m/z* 739 and 553 are formed from the loss of one biphytanyl chain with two

cyclopentyl moieties. The structure and the formation of product ions from loss of the biphytanyl chain are also shown.

Fig. 5. UHPLC-APCI-MS chromatogram shown as EIC, illustrating brGDGTs in the apolar fraction of sample M84/1 GeoB15103-2, 21-34 cmbsf. Several additional compounds with the same molecular mass as the original brGDGTs are separated after analysis with the tandem method, but not all peaks are fully separated. Roman numbers refer to structures presented by Weijers et al. (2007). Compounds are labeled with *m/z* of the molecular ion.

Fig. 6. UHPLC-APCI-MS^2 spectrum of GDGT-1 and GDGT-1a in sample M84/1 GeoB15103-2, 21-34 cmbsf. Shown are the MS^2 fragment ions of the tetraether core ($[M+H]^+$ ion of *m/z* 1300.3) in the range *m/z* 500-1310. The structure of GDGT-1 and the formation of the major fragments are also shown. The enlarged area highlights the main cluster of fragments. The cluster is characterized by multiple losses of water (18.0 Da) and glycerol-derived $C_3H_6O_2$ units (74.0 Da).

Fig. 7. UHPLC-APCI-MS^2 spectrum of GDGT-2 and GDGT-2a in sample M84/1 GeoB15103-2, 21-34 cmbsf. Shown are the MS^2 fragment ions of the tetraether core ($[M+H]^+$ at *m/z* 1298.3) within the *m/z* range 500 - 1310. The enlarged area shows fragments produced by losing one biphytanyl moiety. Both spectra show fragments of a combination of two monocyclic biphytanes vs. an acyclic/bicyclic biphytane combination. The structure and the formation of product ions by loss of one biphytanyl moiety are also shown.

Fig. 8. UHPLC-APCI-MS^2 spectrum of GDD-2 and GDD-2a in sample M84/1 GeoB15103-2, 21-34 cmbsf. Shown are the MS^2 fragment ions of the diether core ($[M+H]^+$ at *m/z* 1242.3) within the *m/z* range 500-1310. The structure of GDD-2 and the formation of the major fragment are also shown. The enlarged area highlights the main cluster of fragments. The cluster is characterized by multiple losses of water (18.0 Da) and glycerol-derived $C_3H_6O_2$ units (74.0 Da). Both spectra show fragments of a combination of two monocyclic biphytanes vs. an acyclic/bicyclic biphytane combination.

Fig. 9. EIC showing the distribution of brGDGT-III isomers in the sample from the Aarhus Bay, 6-7 mbsf. Below: UHPLC-APCI-MS^2 mass spectra of brGDGT-III isomers (a-f) and the formation of the major product ions of the tetraether core ($[M+H]^+$ at *m/z* 1050.0) within the *m/z* range 400-1060 are shown. The enlarged area highlights the main cluster of fragments of the peaks c and f. Both spectra are characterized by the loss of an alkyl moiety

525 and additional, multiple losses of water and glycerol-derived $C_3H_6O_2$ units (74.0 Da). Additionally, the MS^2
526 spectrum of peak c shows two major series of fragment ions indicating that the peak is a mixture of at least two
527 compounds with different total carbon numbers in the alky chain, one having a combination of a C_{30} and a C_{32}
528 alkyl chain and one having a combination of two C_{31} alkyl chains, whereas the MS^2 spectrum of peak f only
529 shows one series of fragments indication a structure with identical total carbon numbers in the alkyl chains
530 (C_{31}). Also shown are possible structures for the isomers and the formation of their major product ions.

531 **TABLES**

532 **Table 1**

533 Sample site characteristics.

Cruise	Site	Location	Position	Water depth (m)	Sampling interval (cmbsf)
M84/1	GeoB15103	Eastern Mediterranean	34°01.65'N/32°37.80'E	1367	21-34
M84/1	GeoB15104	Sea of Marmara	40°47.97'N/27°43.49'E	600	360-375
M84/1	GeoB15105	Black Sea	41°31.71'N/30°53.07'E	1266	425-435

534

Table 2

Chromatographic resolution calculated after Eq. (1) of critical pairs of isoprenoid GDGTs, brGDGTs and GDDs in sample GeoB15103-2, 21-34 cmbsf determined by replicate analysis with different columns. No values are reported for resolutions < 0.5 (-) because peaks cannot be integrated correctly below this value.

Method	GDGT-1 /GDGT-1a	GDGT-2 /GDGT-2a	GDGT-3 /GDGT-3a	GDGT-4 /GDGT-5	GDGT-5 /GDGT-5'	brGDGT-I /brGDGT-1a	brGDGT-Ia /brGDGT-1b	GDD-1 /GDD-1a	GDD-2 /GDD-2a	GDD-3 /GDD-3a	GDD-4/ GDD-5a
1[a] (n=2)	0.69±0.01	0.73±0.02	0.59±0.04	-	1.85±0.14	1.24±0.06	1.47±0.13	-	0.51±0.02	-	-
2[b] (n=2)	0.73±0.01	0.73±0.02	0.60±0.02	0.55±0.03	1.36±0.10	1.62±0.02	1.96±0.05	0.67±0.06	1.10±0.01	-	0.83±0.09
3[c] (n=3)	1.08±0.06	1.16±0.03	0.65±0.01	0.83±0.05	2.04±0.08	1.83±0.06	1.98±0.03	0.81±0.12	1.17±0.08	0.51±0.04	0.84±0.12

[a] Prevail Cyano column, 3 µm particle size;

[b] Acquity BEH HILIC amide column, 1.7 µm particle size, 150 mm length;

[c] two Acquity BEH HILIC amide columns in tandem, 1.7 µm particle size, 150 mm length each.

Table 3

TEX^{H}_{86} obtained from the different methods.

Method	Site, sample	Values excluding shoulders TEX^{H}_{86}	Values including shoulders TEX^{H}_{86}
1[a]	GeoB15103, 21-34 cmbsf	-0.16±0.0043	-0.10±0.0026
2[b]		-0.16±0.0041	-0.09±0.0042
3[c]		-0.16±0.0029	-0.10±0.0013
1[a]	GeoB15104, 360-375 cmbsf	-0.39±0.0007	-0.39±0.0040
2[b]		-0.38±0.0016	-0.37±0.0010
3[c]		-0.37±0.0006	-0.36±0.0029
1[a]	GeoB15105, 420-435 cmbsf	-0.28±0.0071	-0.27±0.0078
2[b]		-0.27±0.0050	-0.26±0.0035
3[c]		-0.26±0.0075	-0.25±0.0072

[a] Prevail Cyano column, 3 µm particle size;

[b] Acquity BEH HILIC amide column, 1.7 µm particle size, 150 mm length;

[c] two Acquity BEH HILIC amide columns in tandem, 1.7 µm particle size, 150 mm length each.

Table 4

Relative abundance obtained with the tandem method for the major GDGT groups in the apolar fraction of the three samples (numbers in brackets represent % within the groups of isoprenoid GDGTs, brGDGTs and GDDs, respectively; n.d., not detected).

		Apolar fraction		
	GDGT or GDD	GeoB15103 21-34 cmbsf	GeoB15104 360-375 cmbsf	GeoB15105 425-435 cmbsf
Relative abundance of isoprenoid GDGTs (%)	0	21.8 (26.2)	18.4 (27.7)	21.8 (30.1)
	1a	1.0 (1.2)	0.4 (0.6)	0.4 (0.6)
	1	6.8 (8.1)	7.2 (10.9)	8.7 (12.0)
	2a	3.4 (4.1)	0.3 (0.4)	0.4 (0.6)
	2	10.5 (12.6)	4.3 (6.5)	8.7 (12.1)
	3a	0.4 (0.4)	0.1 (0.2)	0.1 (0.2)
	3	1.1 (1.3)	0.6 (1.0)	1.3 (1.8)
	4a	0.1 (0.1)	n.d.	n.d.
	4	0.5 (0.6)	0.5 (0.8)	0.3 (0.5)
	5	34.2 (41.0)	34.3 (51.4)	30 (41.4)
	5'	3.6 (4.4)	0.4 (0.6)	0.5 (0.7)
Relative abundance of brGDGTs (%)	III	1.5 (15.1)	5.5 (33.2)	3.7 (27.0)
	IIIa	0.2 (1.9)	1.4 (8.6)	0.8 (5.6)
	IIIb	0.0 (0.3)	0.2 (1.4)	0.1 (1.0)
	II	2.4 (24.7)	3.7 (22.1)	2.9 (21.2)
	IIa	0.4 (4.4)	1.6 (9.7)	2.9 (21.0)
	IIb	0.1 (0.7)	0.2 (1.1)	0.5 (3.8)
	I	4.3 (44.4)	3.3 (19.9)	1.2 (8.5)
	Ia	0.6 (6.7)	0.5 (3.1)	1.1 (8.3)
	Ib	0.2 (1.8)	0.1 (0.9)	0.5 (3.5)
Relative abundance of isoprenoid GDDs (%)	0	1.4 (25.2)	1.7 (24.4)	1.5 (24.9)
	1a	0.2 (3.7)	0.4 (5.4)	0.4 (6.1)
	1	0.2 (3.9)	0.4 (5.5)	0.4 (5.9)
	2a	0.3 (5.9)	0.3 (4.0)	0.4 (5.9)
	2	0.2 (3.4)	0.2 (2.7)	0.3 (4.5)
	3a	0.1 (1.0)	0.1 (0.8)	0.1 (1.0)
	3	0.1 (1.0)	0.0 (0.7)	0.1 (1.1)
	4a	0.0 (0.3)	0.0 (0.4)	0.0 (0.4)
	4	0.1 (0.9)	0.1 (0.7)	0.1 (0.8)
	5a	1.0 (17.4)	1.5 (21.2)	1.1 (17.7)
	5	2.1 (37.2)	2.4 (34.3)	2.0 (31.8)

Figure 1

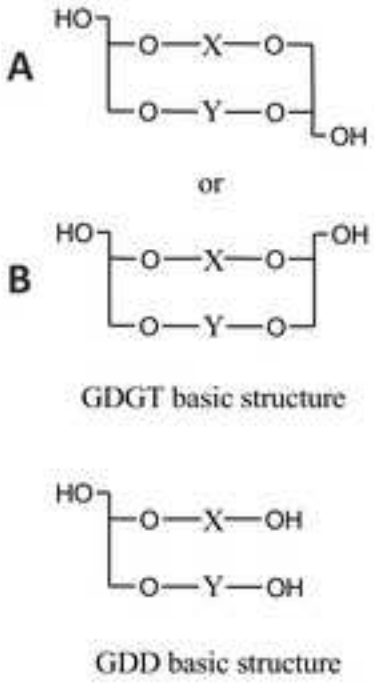

GDGT no.	X	Y	GDGT basic structure	Number of isomers
0	a	a	A, B	2
1	a	b	A, B	4
1	b	a	A, B	
2	b	b	A, B	
2	b	b'	A, B	
2	b'	b	A	8
2	a	c	A, B	
2	c	a	B	
3	b	c	A, B	
3	b'	c	A	
3	c	b	B	
3	a	d	A, B	12
3	d	a	A, B	
3	a	e	A, B	
3	e	a	A, B	
5	c	f	A, B	4
5	f	c	A, B	

GDD no.	X	Y	Number of isomers
0	a	a	1
1	a	b	4
1	a	b'	
1	b	a	
1	b'	a	
2	b	b	6
2	b	b'	
2	b'	b	
2	b'	b'	
2	a	c	
2	c	a	
3	b	c	12
3	b'	c	
3	c	b	
3	c	b'	
3	a	d	
3	a	d'	
3	d	a	
3	d'	a	
3	a	e	
3	a	e'	
3	e	a	
3	e'	a	
5	c	f	4
5	c	f'	
5	f	c	
5	f'	c	

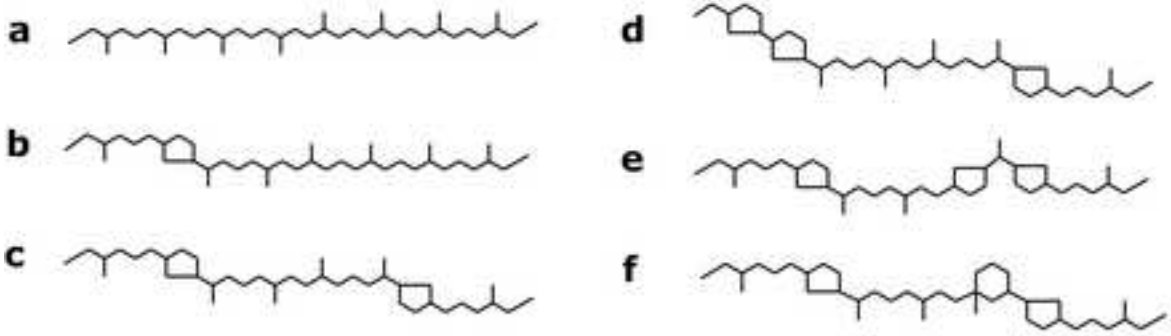

Figure 2

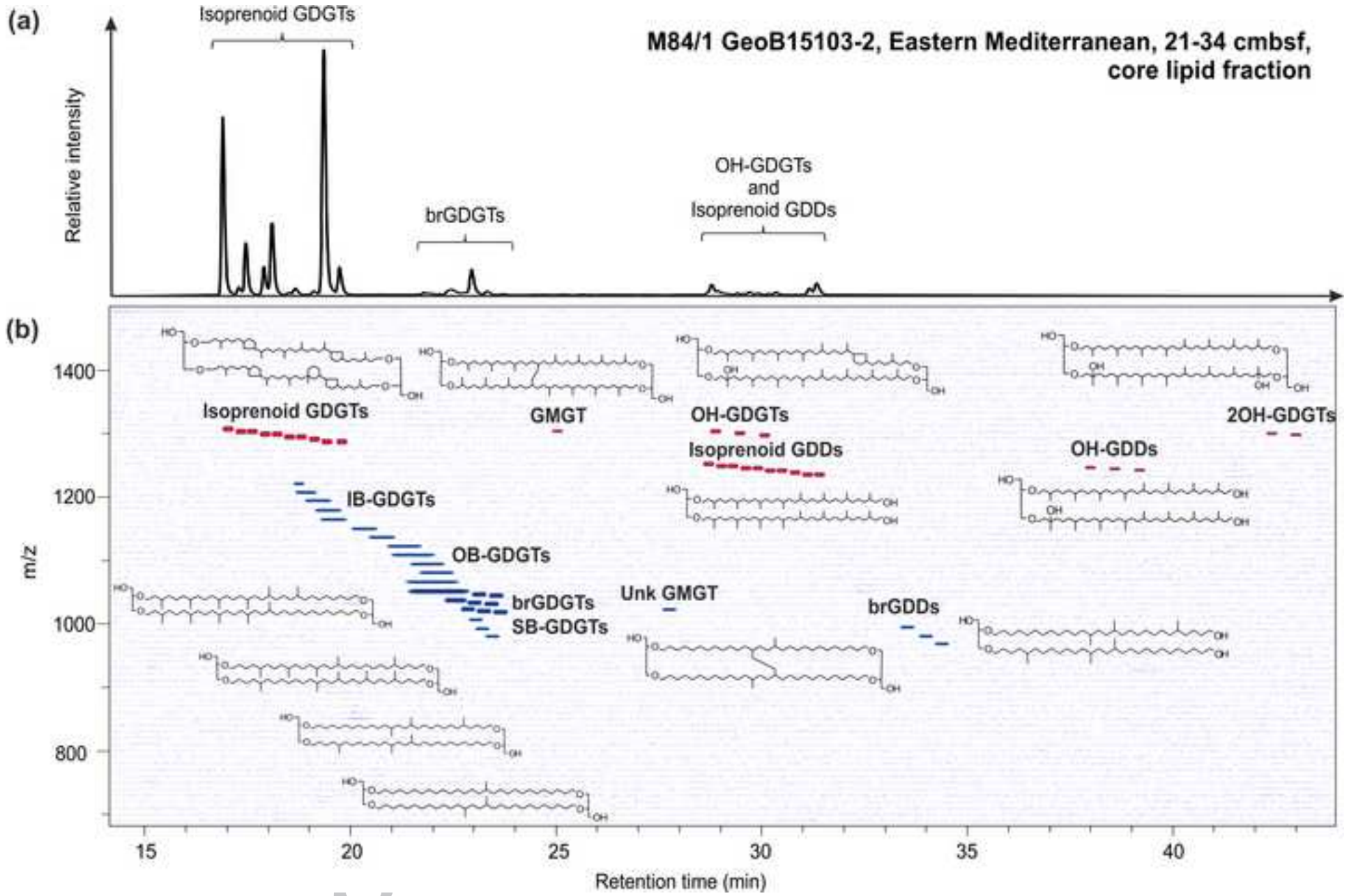

Figure 3

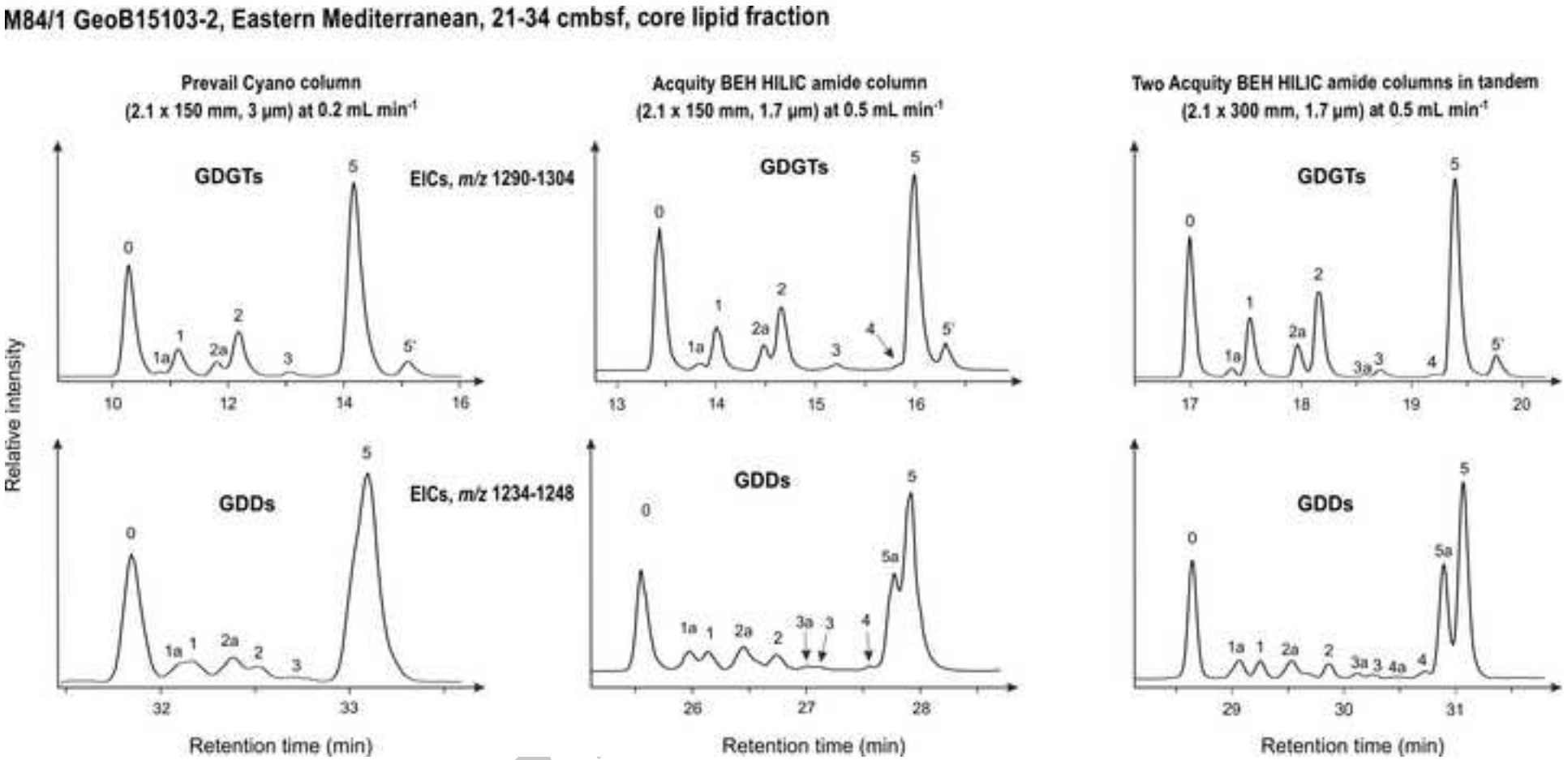

Figure 4

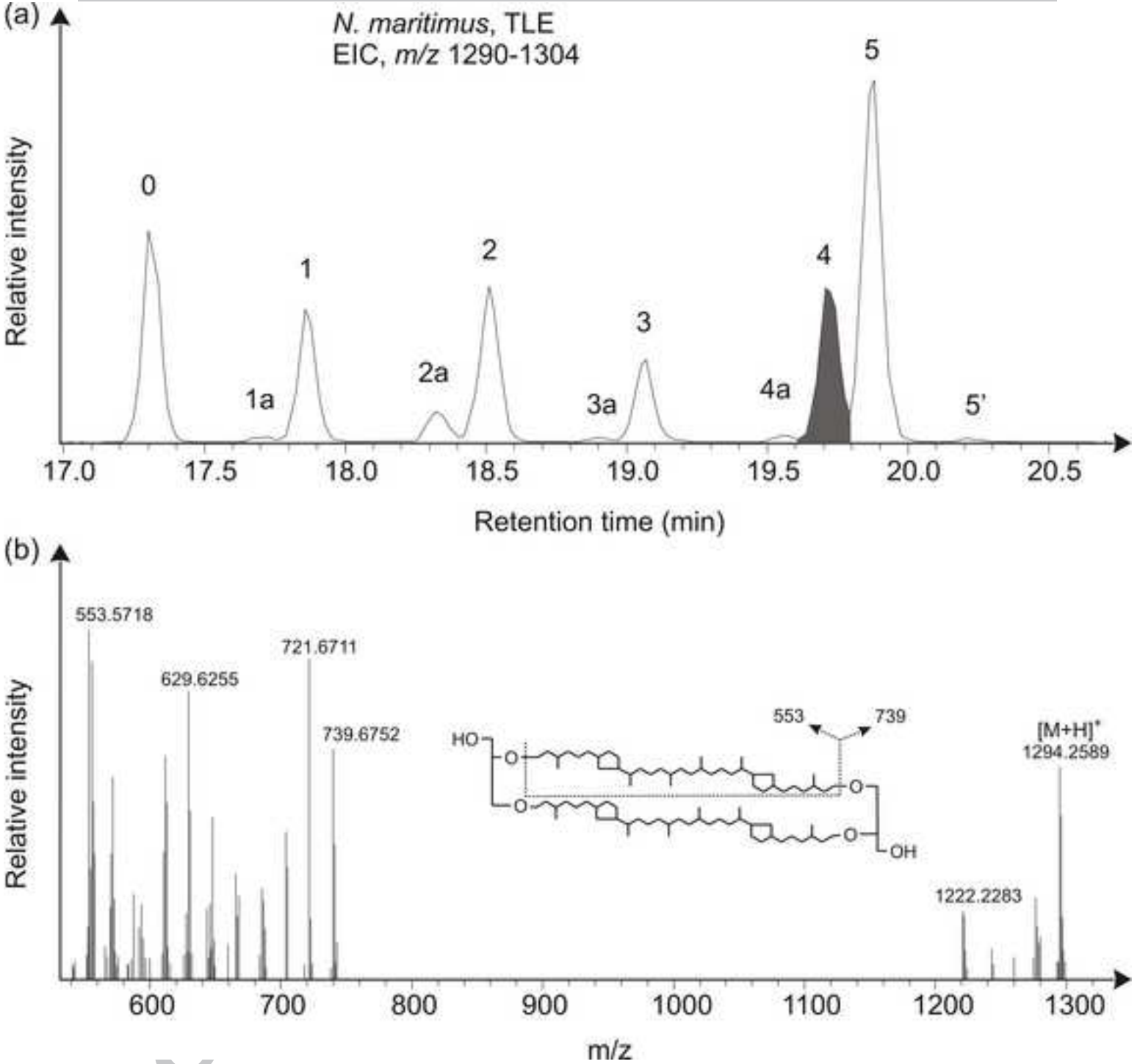

Figure 5

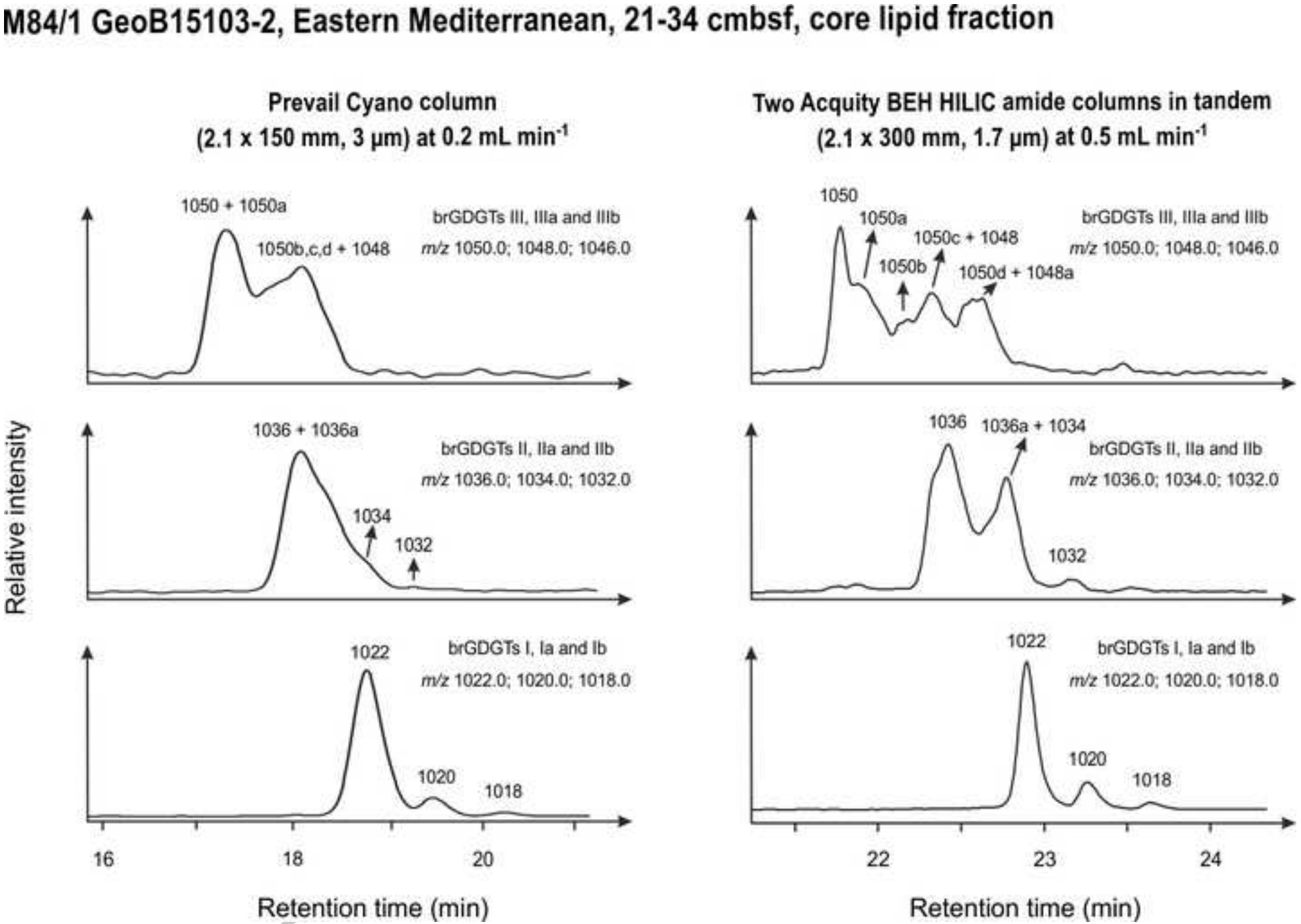

Figure 6

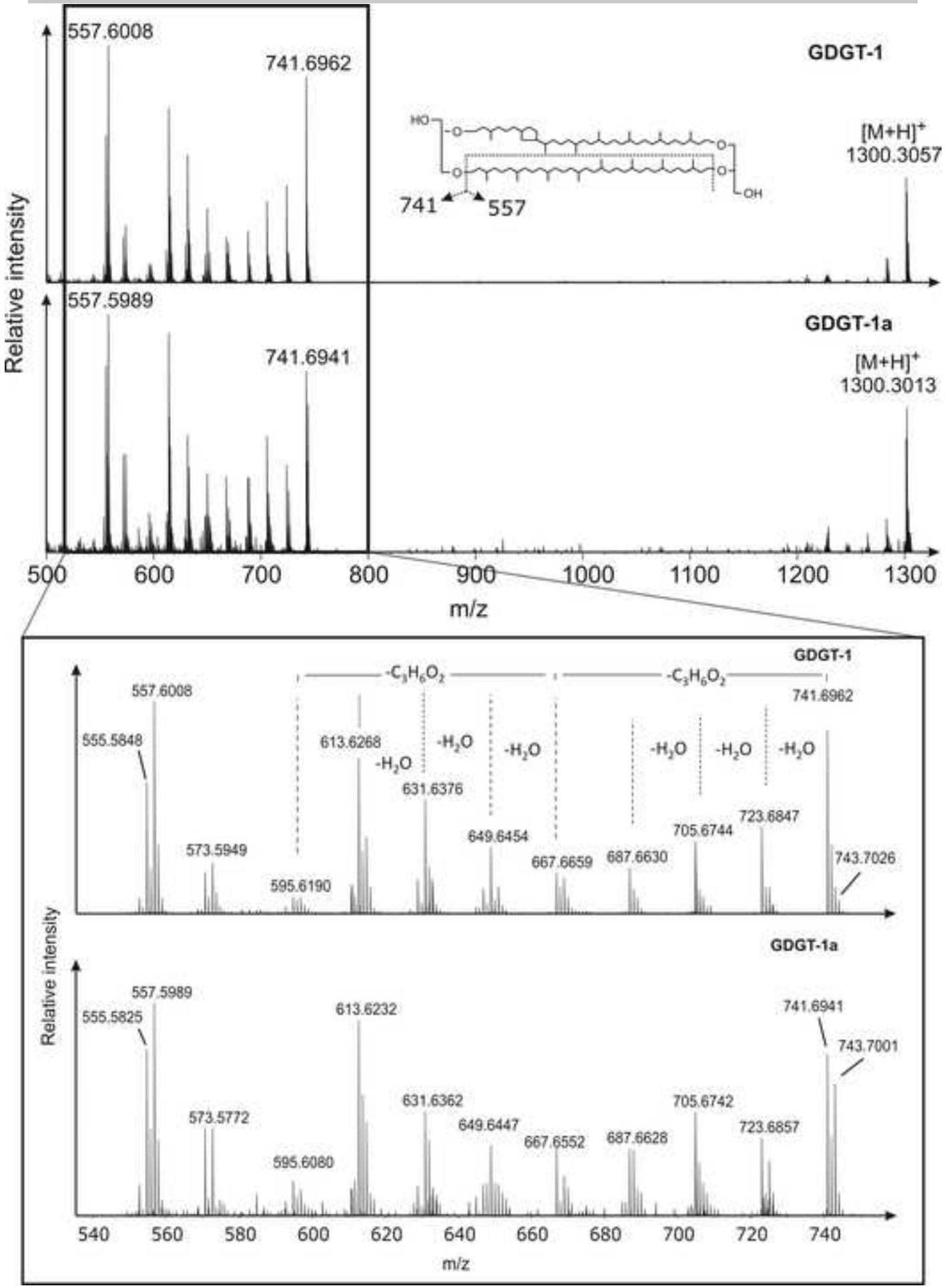

Figure 7

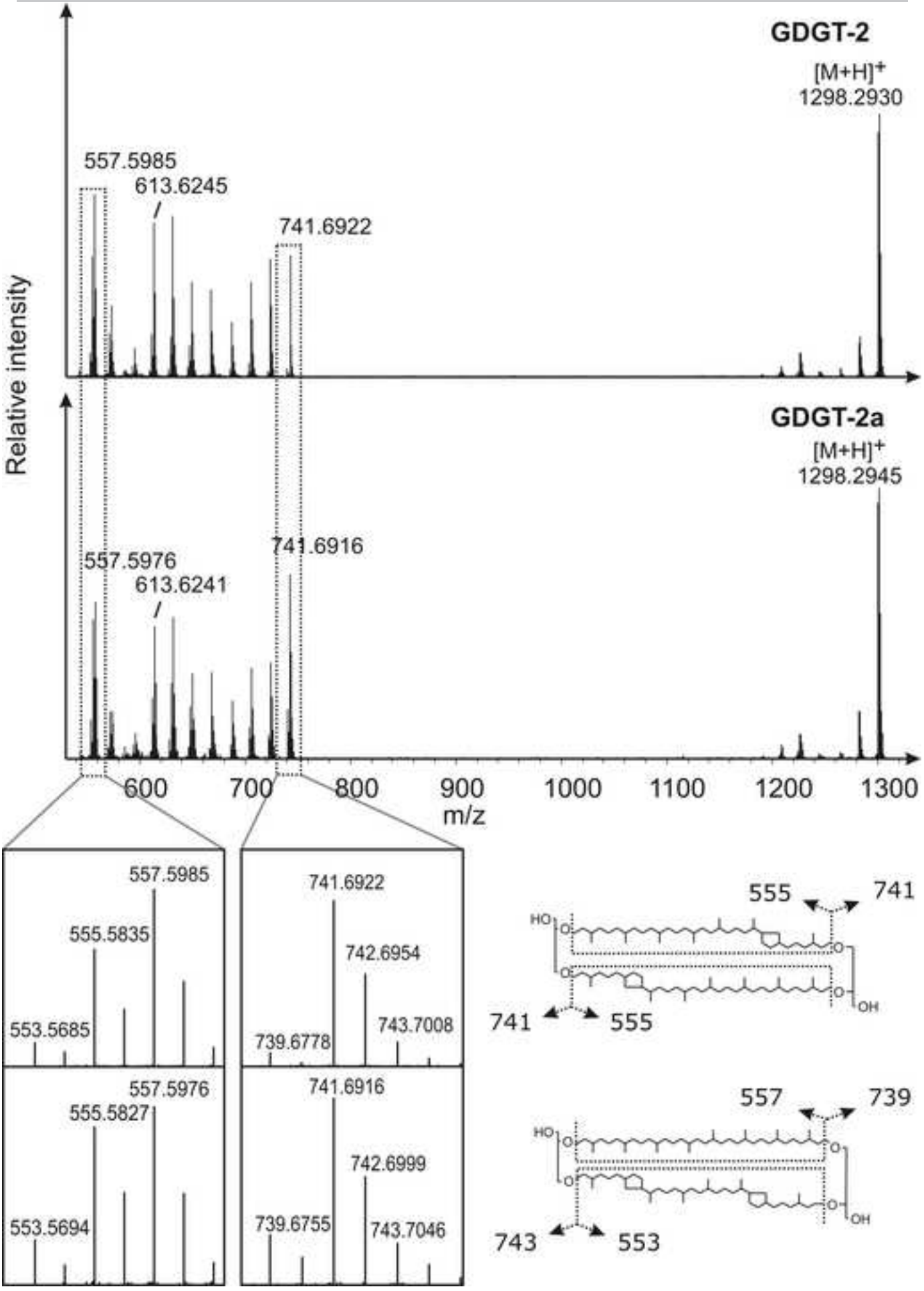

Figure 8

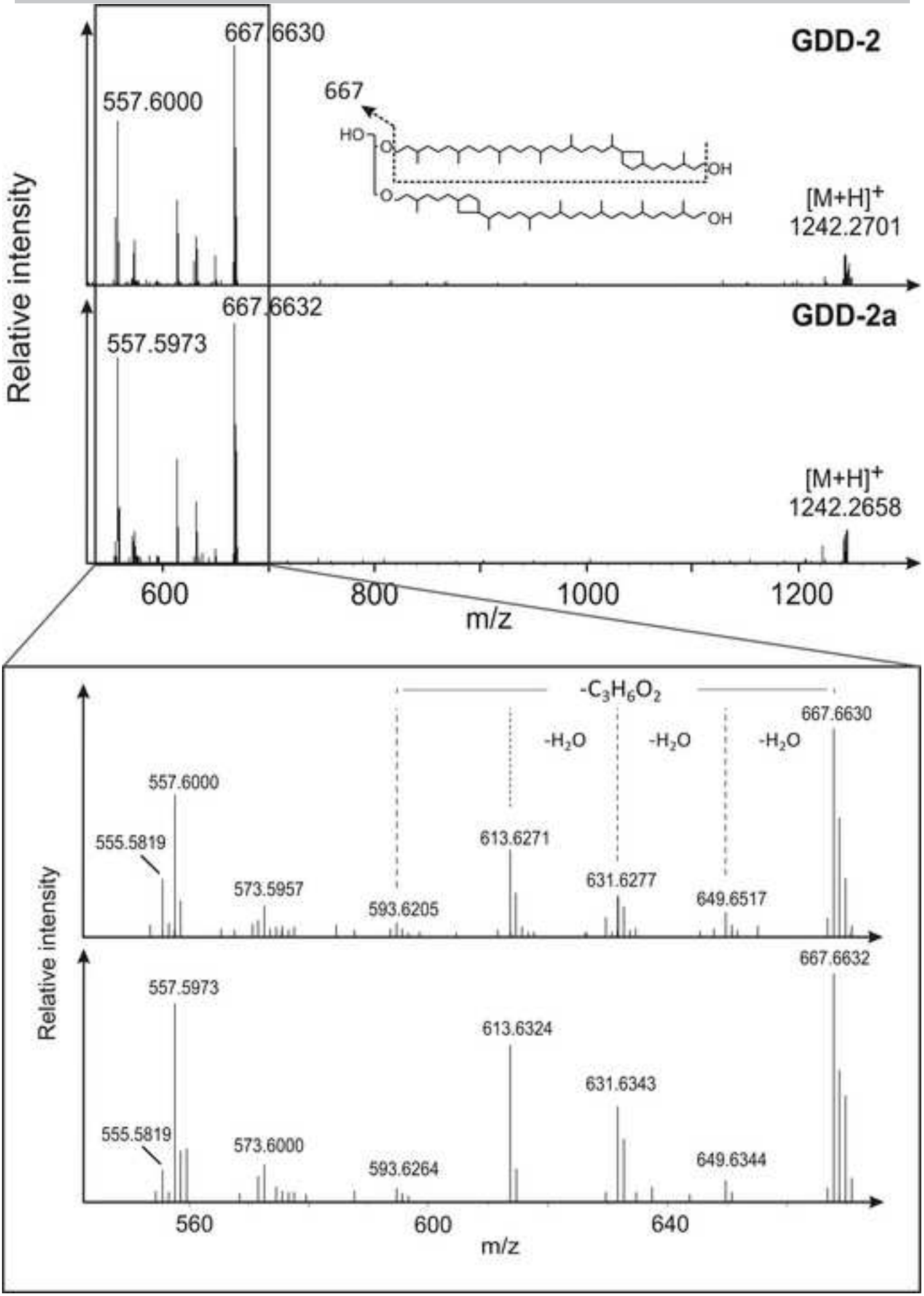

Figure 9

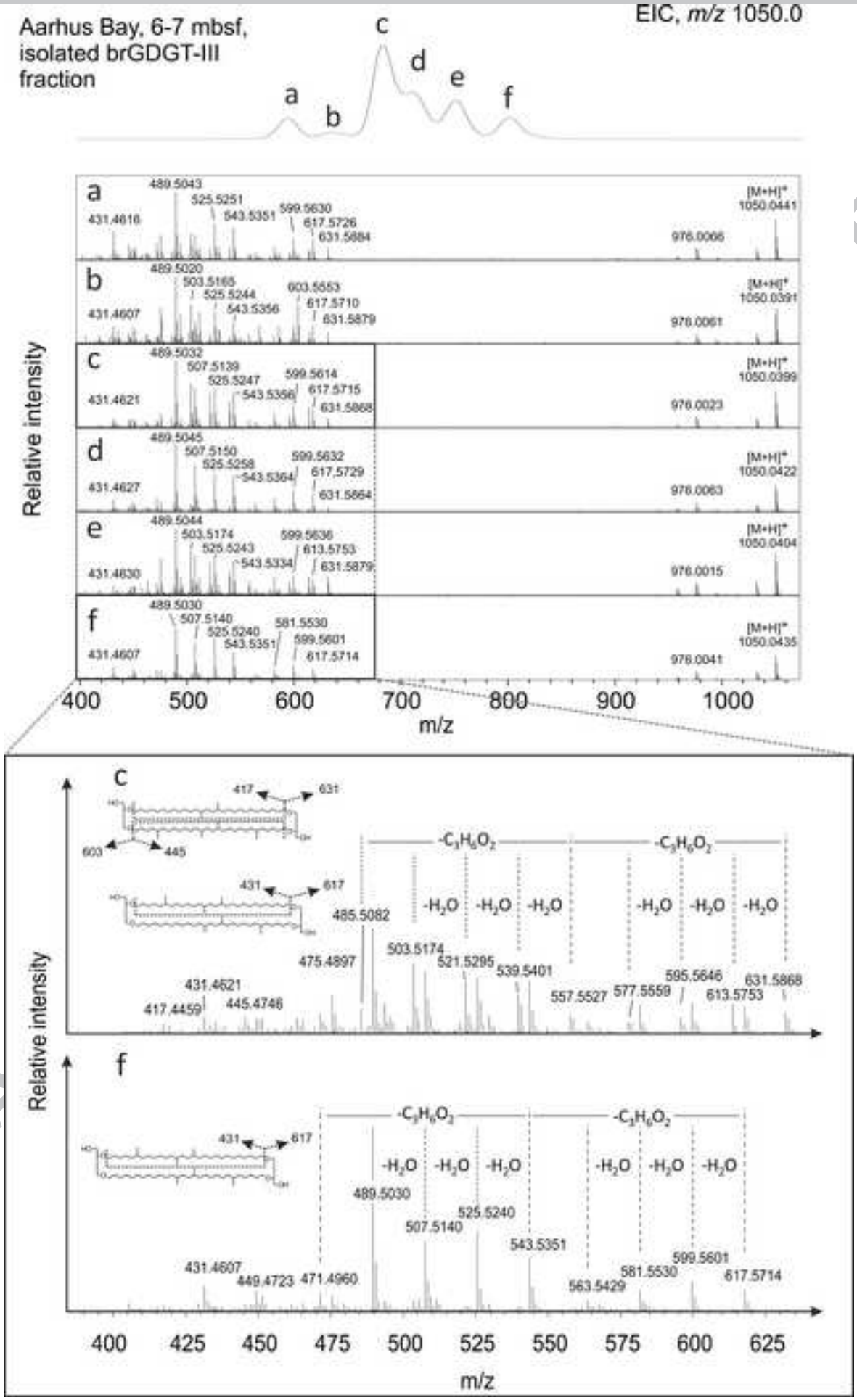

Highlights

- A new UHPLC/APCI-MS protocol for ether core lipid analysis is described.
- It enables separation of previously co-eluting, unidentified GDGT isomers.
- Provides more nuanced exploration of environmental distributions of archaeal and bacterial ether lipids.
- Annotated mass spectra of various isomers are presented.